Enhanced Multi-MeV Photon Emission by a Laser-Driven Electron Beam in a Self-Generated Magnetic Field

D. J. Stark,[1] T. Toncian,[2] and A. V. Arefiev[1,2]

[1]*Institute for Fusion Studies, The University of Texas, Austin, Texas 78712, USA*
[2]*Center for High Energy Density Science, The University of Texas at Austin, Austin, Texas 78712, USA*
(Received 4 November 2015; published 6 May 2016)

We use numerical simulations to demonstrate that a source of collimated multi-MeV photons with high conversion efficiency can be achieved using an all-optical single beam setup at an intensity of 5×10^{22} W/cm^2 that is already within reach of existing laser facilities. In the studied setup, an unprecedented quasistatic magnetic field (0.4 MT) is driven in a significantly overdense plasma, coupling three key aspects of laser-plasma interactions at high intensities: relativistic transparency, direct laser acceleration, and synchrotron photon emission. The quasistatic magnetic field enhances the photon emission process, which has a profound impact on electron dynamics via radiation reaction and yields tens of TW of directed MeV photons for a PW-class laser.

The rapid improvement in ultraintense laser pulses has unlocked new areas of physics, both in fundamental research and technological applications. The prospect of generating copious quantities of multi-MeV photons in laser-target interactions has recently attracted particular interest due to its many potential applications, including pair production [1], laboratory astrophysics [2], photonuclear spectroscopy [3,4], radiation therapy [5], and radiosurgery [6].

Presently, Compton backscattering is one of the primary means for gamma-ray generation, combining conventional electron acceleration with laser technology [7]. Several laser facilities are due to be commissioned in the next few years that are expected to operate at intensities beyond 10^{23} W/cm^2 and that will potentially enable all-optical gamma-ray sources [8,9]. Such high intensities would also give rise to a novel regime of laser-matter interactions in which radiation reaction significantly impacts the particle dynamics. In this regime, the combination of the ultraintense fields and the ultrarelativistic electrons generated by the laser would lead to copious emission of multi-MeV photons. The prospects of reaching this regime have stimulated numerous analytical and numerical studies on gamma-ray production at these high laser intensities [10–16]. Nevertheless, one would have to wait until the intensities exceeding 10^{23} W/cm^2 are achieved in order to implement any of the proposed all-optical photon generation schemes.

There are, however, several facilities with the capability of reaching intensities up to 5×10^{22} W/cm^2 within the immediate future [17]. Most of the previous numerical studies have concluded that synchrotron emission shows little promise for converting an appreciable fraction of laser energy into high-energy photons at laser intensities below 10^{23} W/cm^2 for PW-class laser systems [12,16]. It was concluded that an order of magnitude increase of either laser intensity or laser power would be required to achieve tens of percent for the total conversion rate and for radiation reaction effects to become pronounced.

In this Letter, we use 2D and 3D particle-in-cell (PIC) simulations to perform a numerical study of photon emission from laser-irradiated solid-density bulk targets using a PW-class pulse of intensity 5×10^{22} W/cm^2. We demonstrate that a MT-level quasistatic magnetic field generated by collective effects in a relativistically transparent laser-heated plasma facilitates sustained electron acceleration and consequently enhances the photon emission rate, yielding tens of TW of directed MeV photons for a PW-class laser system. Remarkably, the resulting laser energy conversion rate for multi-MeV photons is comparable to that previously predicted for an order of magnitude higher in intensity or power. Additionally, we propose a novel target geometry to control the directionality of this high-yield photon beam.

The synchrotron emission is expected to be the primary source of multi-MeV photons at this laser intensity. The emission process of hard photons must be calculated self-consistently by explicitly accounting for the radiation reaction in the description of the electron dynamics. A probabilistic approach based on classical and QED synchrotron cross sections, coupled with the subsequent reduction of the electron momentum [11], has been successfully implemented in the fully relativistic PIC code EPOCH [18,19] that we use in this study.

As the first step in our study, we examined how solid, thick targets perform when irradiated at normal incidence by a pulse with characteristics similar to those of the Texas Petawatt [17]. We have performed 2D PIC simulations for several different target densities while using the same 5×10^{22} W/cm^2 PW-class laser pulse. Specifically, we

used a 1 μm wavelength, linearly polarized (electric field in the simulation plane) Gaussian pulse that is 100 fs in duration and that focuses to a spot 1.1 μm in radius. The peak normalized wave amplitude that corresponds to 5×10^{22} W/cm^2 for this pulse is $a_0 \approx 190$. We initialized the targets as fully ionized uniform carbon plasmas with electron densities ranging from $n_e \approx 4.5n_c$ to $n_e \approx 110n_c$, which in practice corresponds to foam and plastic targets. Here $n_c = 1.1 \times 10^{21}$ cm^{-3} is the critical density. The cell size was 10×10 nm with 20 to 50 electrons and 10 to 20 ions per cell.

The density decrease in the considered range describes the transition from the relativistically near-critical regime to the relativistically transparent regime. As shown in Fig. 1, for the higher densities the laser penetration into the target is only due to stable hole boring [20,21], whereas at the lower densities the laser pulse propagates through the target due to the relativistically induced transparency [22]. The density scan shows that the yield of multi-MeV photons increases with the onset of relativistic transparency.

The relativistically transparent targets demonstrate enhanced performance beyond just the overall yield of the multi-MeV photons. For the near-critical target, the photons are emitted by both forward and backward-moving electrons, as shown in Fig. 1(f). This leads to a low degree of collimation [see Fig 1(g)]. In the relativistically transparent regime, the emission pattern dramatically changes for higher energy photons. For energies above 10 MeV, the photons are emitted almost exclusively by

forward-moving electrons [panel (d)]; this directly translates into a highly collimated multi-MeV photon beam [panel (e)]. The key features of relativistically transparent targets, then, are the increased efficiency and the dramatically enhanced collimation of the photon beam.

However, these advantages are gained at the cost of the directivity of the photon beam. The laser beam propagation in the relativistically transparent regime is unstable. As the laser pulse veers off its axis [see Fig 1(a)], so will the energetic electrons accelerated by the pulse. Since these electrons essentially emit parallel to their momentum, the directivity of the photon beam becomes just as unpredictable, as indicated in Fig. 1(e).

In order to utilize the best features of both regimes, we propose a novel target design shown in Fig. 2 that combines a relativistically near-critical (100 n_c) bulk target and a relativistically transparent (10 n_c) channel. The 0.9 μm channel radius was chosen to optimize laser coupling into the channel [23]. Figure 2(b) confirms that, similarly to the case of bulk relativistically transparent targets, the high energy photons are predominantly emitted by forward-moving electrons. This leads to a well-collimated photon beam [panel (c)] with a high conversion efficiency of ∼15%. What is more significant is that the near-critical bulk target guides the laser pulse so that the resulting photon beam is symmetric and directed along the axis of the channel. An intensity scan shows that these features are robust, with the efficiency remaining above 1% for multi-MeV photons at intensities above 10^{22} W/cm^2 (see S2 in
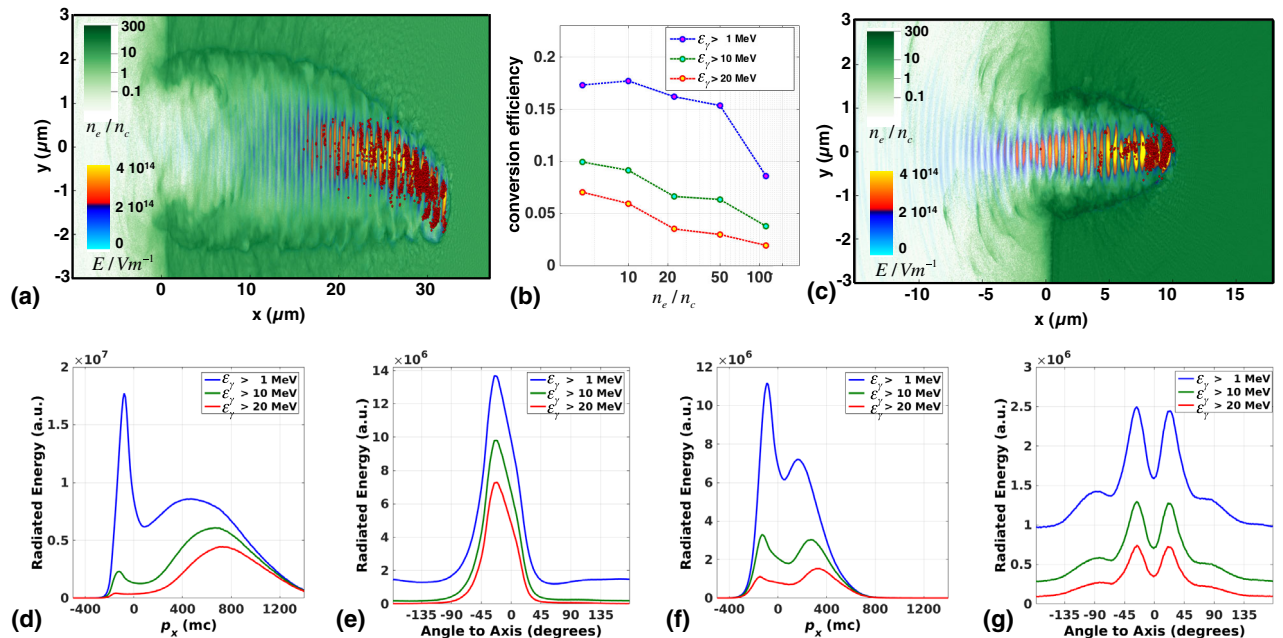

FIG. 1. Results of 2D simulation density scan measuring the conversion efficiency of laser energy into gamma rays [panel (b)] with energies above 1, 10, and 20 MeV. Panels (a) and (c) show density and electric field snapshots for $n_e = 10n_c$ at 300 fs and $n_e = 50n_c$ at 250 fs, with photon emissions greater than 10 MeV in energy denoted by red circles. The time-integrated radiated energies for these two simulations are shown as functions of emitting electron longitudinal momentum [(d) and (f)] and the angle of emission relative to the laser's initial propagation axis [(e) and (g)].
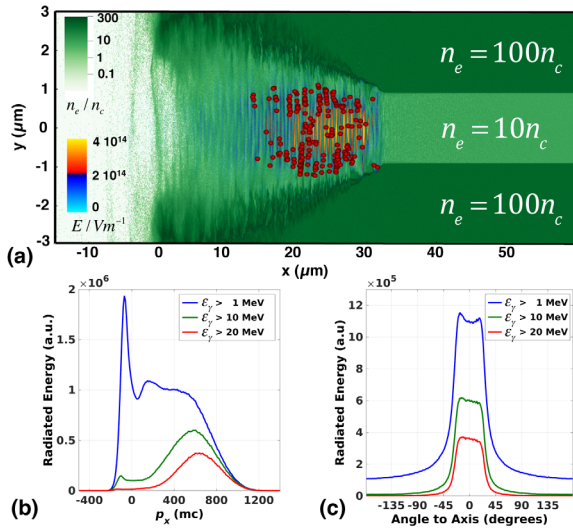
FIG. 2.   Density and electric field snapshot from the 2D channel simulation at 300 fs (a), where photon emissions greater than 10 MeV in energy are denoted by red circles. The time-integrated radiated energy in the simulation is shown as a function of emitting electron longitudinal momentum (b) and the angle of emission relative to the laser propagation axis (c).

the Supplemental Material [24]). The number of high energy electrons and photons doubles if the radiation reaction is neglected, which underscores its importance (see S1 in Ref. [24]).

Still, the obtained result is counterintuitive, because it is well known that energetic electrons copropagating with the laser pulse in a vacuum are poor sources of gamma-ray emission. The acceleration induced by the laser is significantly higher for counterpropagating electrons [25,26]. In order to understand the underlying mechanism of the gamma-ray emission in our setup, it is constructive to briefly examine the salient features of the synchrotron emission. The power emitted by a single electron is effectively determined by the acceleration in an instantaneous rest frame, $P_{\rm rad} \propto \eta^2$, where [11,19]

$$\eta = \frac{\gamma}{E_S} \sqrt{\left(\mathbf{E} + \frac{1}{c}[\mathbf{v} \times \mathbf{B}]\right)^2 - \frac{1}{c^2}(\mathbf{E} \cdot \mathbf{v})^2}. \quad (1)$$

Here, $\mathbf{E}$ and $\mathbf{B}$ are the electric and magnetic fields acting on the electron, γ and $\mathbf{v}$ are the relativistic factor and velocity of the electron, and $E_S \approx 1.3 \times 10^{18}$ V/m is the Schwinger limit. The parameter η effectively compares the strength of the electric field in the electron's rest frame to E_S. In our simulations, we typically observe $\eta^2 \approx 3 \times 10^{-3}$ during emissions of multi-MeV photons. For comparison, we first take the maximum electric field in the laser pulse, $E_0 \approx 6 \times 10^{14}$ V/m, and the typical relativistic factor of emitting electrons, $\gamma \approx 700$. Not surprisingly, such a strong field produces tremendous acceleration for a copropagating electron, with $\eta^2 \approx 0.1$. However, the magnetic field of the laser pulse counteracts the force from the electric field. As a

result, the acceleration in the laser pulse drops to $\eta^2 \approx 10^{-13}$ for an electron moving in the same direction as the pulse. We must note, though, that the electric field of the pulse does cause transverse oscillations, with a typical angle of 20° for the emitting electrons as they cross the channel's axis. Even in this case, $\eta^2 \approx 4 \times 10^{-4}$ and so is still an order of magnitude lower than what is observed in the simulations. The laser-plasma interaction itself must provide an additional contribution to the electromagnetic field that enhances the photon emission.

A comparison of the electric [Fig 2(a)] and magnetic [Fig 3(a)] field snapshots in the channel reveals the presence of a strong magnetic field generated by the electron current, clearly visible near the edges of the channel. The maximum magnetic field that the channel electrons can generate can be estimated as

$$B \approx \frac{4\pi}{c}|e|n_e cR \approx 6 \times 10^5 \text{ T}, \quad (2)$$

where we assume that the electron density n_e is roughly the channel electron density and that R is the channel radius. This expression further assumes that all of the electrons are moving forward with relativistic velocities, whereas in reality, some electrons move under an angle with respect to the channel axis. Though Eq. (2) consequently overestimates the electron current and the corresponding magnetic field, it provides an order-of-magnitude estimate, $B \approx 0.3B_0$, that is comparable to the $\sim 0.2B_0$ that we observe in the simulation. Here, $B_0 \approx 2 \times 10^6$ T is the magnetic field of the wave. We therefore can draw two
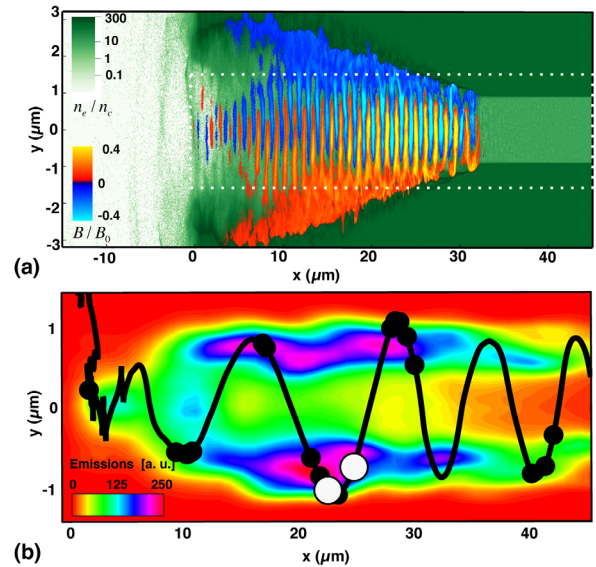

FIG. 3.   (a) Magnetic field B_z and electron density snapshot at 300 fs from the 2D channel simulation. (b) Sample emitting electron trajectory (black) showing the emissions above 2 MeV (black circles) and above 30 MeV (white circles) as it traverses the channel. The background color plot gives the emission count per cell for photons greater than 30 MeV.

important conclusions. First, the estimate indicates that the slowly changing magnetic field is generated by the bulk electrons in the channel. Of greater significance, however, is that the plasma can sustain a magnetic field whose strength is comparable to that of the laser pulse.

The strong self-generated magnetic field considerably increases the acceleration experienced by the electrons moving along the channel. The crucial point is that the force exerted by such a magnetic field is not compensated by an electric field, as in the case of the laser pulse. At $a_0 = 190$, the relativistically corrected electron response time becomes comparable to that for the ions, thus preventing formation of a strong transverse quasistatic electric field. For the characteristic strength of the self-generated magnetic field of $B \sim 0.2B_0$, we have $\eta^2 \approx 4 \times 10^{-3}$, consistent with the values observed in the simulations (see S3 in the Supplemental Material [24]). This attests to the enhancement of the gamma-ray emission in the channel being directly linked to the presence of a strong self-generated magnetic field.

We illustrate this effect of the self-generated field by analyzing the emission pattern along a typical electron trajectory shown in Fig. 3(b) (black line). We chose an electron whose γ factor during the emissions of multi-MeV photons is near the well-pronounced peak shown in Fig. 2(b). After being injected into the channel, the electron is accelerated in the forward direction by the intense laser pulse. The laser electric field drives strong transverse oscillations, while the magnetic field generated by the plasma confines the electron inside the channel. The deflections by the magnetic field of the channel result in emissions of multi-MeV photons, and that is why most of the emissions occur in the vicinities of the turning points. This pattern is evident along the trajectory, where we show the locations of photon emissions with energies above 2 MeV and specifically highlight the photon emissions with energies above 30 MeV.

Furthermore, the emission locations along this electron trajectory are representative of where the bulk of the radiating electrons emit hard photons, as evidenced by the locations of the photon emissions above 30 MeV given in panel (b). The electrons emit at their turning points when they reach the strong quasistatic magnetic field at the edges of the channel, and thus the emissions are localized off axis instead of where the laser fields have the highest amplitude.

In order to make quantitative predictions for the energy conversion rate into multi-MeV photons, we performed a 3D simulation using the same laser pulse parameters and the same target design, now with cylindrical symmetry. We used $23 \times 60 \times 60$ nm cells with 50 electron and 25 ions per cell. The key qualitative features of the laser-target interaction are in good agreement with what has been observed in the 2D case. We recorded the locations and times of the emissions in the simulation and then propagated the photons, as a part of postprocessing, for 1 ps to

observe the far-field distribution (Fig 4). We find that the conversion efficiency into photons with energies above 1 MeV is reduced to 3.5% in the 3D calculation, but the photon divergence out of the plane corresponding to the 2D simulation is significantly smaller than the divergence within that plane [i.e., in the (x, y) plane].

The photon beam is thus more powerful because of the anisotropic divergence than what one would expect when extrapolating the result of the 2D simulation. The beam is also much shorter than the laser pulse, with a characteristic duration of roughly 30 fs for photons with energies above 10 MeV. The photons are emitted in bursts, which leads to very pronounced beam intensity modulations with a periodicity of the laser period. The total number of the multi-MeV photons in the beam is roughly 5.6×10^{12}. Using the calculated conversion efficiency and beam divergence, we expect that the cylindrical channel can effectively convert a PW-class 69 J laser pulse into a multi-TW beam of multi-MeV photons with the total energy exceeding 1 J.

In conclusion, we have examined photon emission from laser-irradiated bulk solid density targets at a laser intensity of 5×10^{22} W/cm^2 through the use of 2D and 3D PIC simulations. We have identified a regime in which a beam of collimated multi-MeV photons can be efficiently generated even at this intensity. In this regime, a quasistatic MT-level magnetic field is driven in the plasma, coupling three key aspects of laser-plasma interactions at high intensities: relativistic transparency, direct laser acceleration, and synchrotron emission. In contrast to the regimes of Refs. [12] and [13], the plasma density must be well below the relativistic critical density. Laser pulse duration
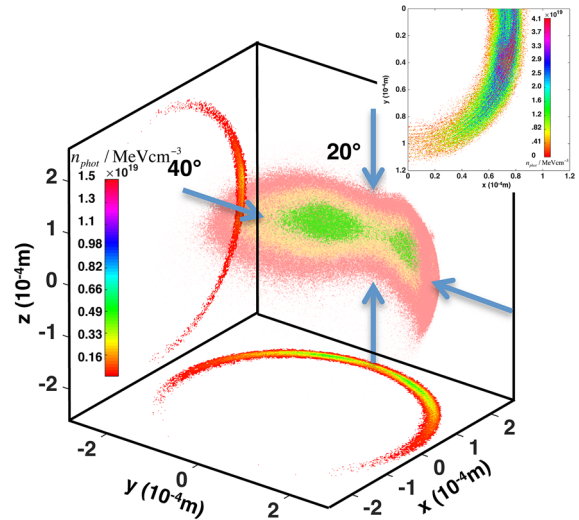

FIG. 4.   Volume plot of the photon energy density as isocontours for 0.2 (green), 0.1 (light yellow), and 0.05 (light red) of the maximum density after 1 ps. On the left and bottom of the box are projections of the planes $(x, 0, z)$ and $(x, y, 0)$, with the angular FWHM of 20° and 40°. The inset shows a central cross section through the (x, y) plane, detailing the temporal substructure of the photon beam after 500 fs.

and plasma density must be such that the strong magnetic field region is sufficiently long to allow forward-moving electrons multiple bounces across the channel. A preformed target geometry with a channel that becomes relativistically transparent during the interaction can control the photon beam directivity and yield tens of TW of directed MeV photons for a PW-class laser. The properties of this emitted photon beam might enable the development of novel applications in areas of imaging, medical treatment, isotope production, and nuclear physics.

---

[1] H. Chen *et al.*, The scaling of electron and positron generation in intense laser-solid interactions, Phys. Plasmas **22**, 056705 (2015).

[2] S. V. Bulanov, T. Zh. Esirkepov, M. Kando, J. Koga, K. Kondo, and G. Korn, On the problems of relativistic laboratory astrophysics and fundamental physics with super powerful lasers, Plasma Phys. Rep. **41**, 1 (2015).

[3] E. C. Schreiber *et al.*, First measurement of the near-threshold $^2H(\vec{\gamma},n)p$ analyzing power using a free-electron laser based γ-ray source, Phys. Rev. C **61**, 061604(R) (2000).

[4] E. Kwan *et al.*, Discrete deexcitations in ^{235}U below 3 MeV from nuclear resonance fluorescence, Phys. Rev. C **83**, 041601(R) (2011).

[5] K. J. Weeks, V. N. Litvinenko, and J. M. J. Madey, The Compton backscattering process and radiotherapy, Med. Phys. **24**, 417 (1997).

[6] B. Girolami, B. Larsson, M. Preger, C. Schaerf, and J. Stepanek, Photon beams for radiosurgery produced by laser Compton backscattering from relativistic electrons, Phys. Med. Biol. **41**, 1581 (1996).

[7] S. Chen *et al.*, MeV-Energy X Rays from Inverse Compton Scattering with Laser-Wakefield Accelerated Electrons, Phys. Rev. Lett. **110**, 155003 (2013).

[8] K. Ta Phuoc, S. Corde, C. Thaury, V. Malka, A. Tafzi, J. P. Goddet, R. C. Shah, S. Sebban, and A. Rousse, All-optical Compton gamma-ray source, Nat. Photonics **6**, 308 (2012).

[9] N. D. Powers, I. Ghebregziabher, G. Golovin, C. Liu, S. Chen, S. Banerjee, J. Zhang, and D. P. Umstadter, Quasi-monoenergetic and tunable X-rays from a laser-driven Compton light source, Nat. Photonics **8**, 28 (2014).

[10] L. L. Ji, A. Pukhov, E. N. Nerush, I. Yu. Kostyukov, K. U. Akli, and B. F. Shen, Near QED regime of laser interaction with overdense plasmas, Eur. Phys. J. Spec. Top. **223**, 1069 (2014).

[11] R. Duclous, J. G. Kirk, and A. R. Bell, Monte Carlo calculations of pair production in high-intensity laser plasma interactions, Plasma Phys. Control Fusion **53**, 015009 (2011).

[12] C. S. Brady, C. P Ridgers, T. D. Arber, A. R. Bell, and J. G. Kirk, Laser Absorption in Relativistically Underdense Plasmas by Synchrotron Radiation, Phys. Rev. Lett. **109**, 245006 (2012).

[13] C. P. Ridgers, C. S. Brady, R. Duclous, J. G. Kirk, K. Bennett, T. D. Arber, A. P. L. Robinson, and A. R. Bell, Dense Electron-Positron Plasmas and Ultraintense γ rays from Laser-Irradiated Solids, Phys. Rev. Lett. **108**, 165006 (2012).

[14] C. S. Brady, C. P Ridgers, T. D. Arber, and A. R. Bell, Synchrotron radiation, pair production, and longitudinal electron motion during 10-100 PW laser solid interactions, Phys. Plasmas **21**, 033108 (2014).

[15] C. S. Brady, C. P. Ridgers, T. D. Arber, and A. R. Bell, Gamma-ray emission in near critical density plasmas, Plasma Phys. Controlled Fusion **55**, 124016 (2013).

[16] T. Nakamura, J. K. Koga, T. Zh. Esirkepov, M. Kando, G. Korn, and S. V. Bulanov, High-Power -Ray Flash Generation in Ultraintense Laser-Plasma Interactions, Phys. Rev. Lett. **108**, 195001 (2012).

[17] M. Martinez *et al.* in *Boulder Damage Symposium XXXVII: Annual Symposium on Optical Materials for High Power Lasers*, edited by G. J. Exarhos, A. H. Guenther, K. L. Lewis, D. Ristau, M. J. Soileau, and C. J. Stolz (SPIE-International Society for Optical Engineering, Bellingham, WA, 2005), p. 59911N.

[18] Extendable PIC Open Collaboration (EPOCH), [Online]. Available: http://ccpforge.cse.rl.ac.uk/gf/project/epoch/.

[19] C. P. Ridgers, J. G. Kirk, R. Duclous, T. G. Blackburn, C. S. Brady, K. Bennett, T. D. Arber, and A. R. Bell, Modelling gamma-ray photon emission and pair production in high-intensity laser matter interactions, J. Comput. Phys. **260**, 273 (2014).

[20] S. C. Wilks, W. L. Kruer, M. Tabak, and A. B. Langdon, Absorption of ultra-intense laser pulses, Phys. Rev. Lett. **69**, 1383 (1992).

[21] A. P. L. Robinson, P. Gibbon, M. Zepf, S. Kar, R. G. Evans, and C. Bellei, Relativistically correct hole-boring and ion acceleration by circularly polarized laser pulses, Plasma Phys. Controlled Fusion **51**, 024004 (2009).

[22] S. Palaniyappan *et al.*, Dynamics of relativistic transparency and optical shuttering in expanding overdense plasmas, Nat. Phys. **8**, 763 (2012).

[23] D. Marcuse, Loss analysis of single-mode fiber splices, Bell Syst. Tech. J. **56**, 703 (1977).

[24] See Supplemental Material at http://link.aps.org/supplemental/10.1103/PhysRevLett.116.185003 for further details of the photon emission and radiation reaction analysis.

[25] T. G. Blackburn, C. P. Ridgers, J. G. Kirk, and A. R. Bell, Quantum Radiation Reaction in Laser Electron-Beam Collisions, Phys. Rev. Lett. **112**, 015001 (2014).

[26] M. Vranic, J. L. Martins, J. Vieira, R. A. Fonseca, and L. Silva, All-Optical Radiation Reaction at 10^{21} W/cm^2, Phys. Rev. Lett. **113**, 134801 (2014).